POLITECNICO DI TORINO
Repository ISTITUZIONALE

The impact of multi-injection events on a compression-ignition engine using ducted fuel injection: A numerical and experimental study

Original
The impact of multi-injection events on a compression-ignition engine using ducted fuel injection: A numerical and experimental study / Orlando, M., Segatori, C., Godbold, C., Mueller, C.J., Millo, F., Piano, A.. - In: FUEL PROCESSING TECHNOLOGY. - ISSN 0378-3820. - ELETTRONICO. - 292:(2026). [10.1016/j.fuproc.2026.108602]

Availability:
This version is available at: 11583/3016023 since: 2026-09-28T13:34:18Z

Publisher:
Elsevier

Published
DOI:10.1016/j.fuproc.2026.108602

Terms of use:

This article is made available under terms and conditions as specified in the corresponding bibliographic description in the repository

Publisher copyright

(Article begins on next page)

26 November 2026

Fuel Processing Technology 292 (2026) 108602

Contents lists available at ScienceDirect

Fuel Processing Technology

journal homepage: www.elsevier.com/locate/fuproc

The impact of multi-injection events on a compression-ignition engine using ducted fuel injection: A numerical and experimental study

M. Orlando [a], C. Segatori [a,*], C. Godbold [b], C.J. Mueller [c], F. Millo [a], A. Piano [a]

[a] Politecnico di Torino, Torino, Italy
[b] The Georgia Institute of Technology, Atlanta, GA, USA
[c] Sandia National Laboratories, Livermore, CA, USA

ARTICLE INFO

Keywords:
Ducted fuel injection
Multi-injection strategies
Optical engine
Computational fluid dynamics
Soot emissions
NOx emissions

ABSTRACT

Ducted fuel injection (DFI) is a technology to curtail soot formation from diesel combustion while mitigating its typical trade-off with nitrogen oxides (NOx). Previous studies have demonstrated its potential in both vessel and compression-ignition (CI) engine applications relying on simple single-injections rather than multi-injection (MI) strategies. Consequently, injection strategy optimization remains an open question. This study examines the interaction between MI strategies and DFI through a combined approach employing analysis of experimental in-vessel data and 3D computational fluid dynamics (CFD) engine simulations.

The analysis was conducted by considering the impact of pilot and post injections on DFI separately, exploring variations in dwell time and mass share. The findings indicate that, when pilot injection is introduced, DFI remains effective in curtailing engine-out soot emissions, while NOx emissions are less sensitive to pilot injection calibration than in free spray injection (FSI). Similarly, post injections can be successfully employed with DFI to further reduce soot emissions, although a different optimal calibration may be required compared to the FSI.

Overall, this study suggests that DFI can be effectively coupled with MI strategies, and that DFI-oriented calibration adjustments may unlock additional benefits, representing a significant step toward its deployment in series-production CI engines.

1. Introduction

In recent years, one of the main focuses in energy research has been the reduction of greenhouse gas (GHG) emissions. The transportation sector is a contributor to global GHG emissions, accounting for approximately one-fifth of the total [1], and various initiatives have been implemented to mitigate this impact. In Europe, for instance, where transportation is responsible for about 25% of total carbon dioxide (CO_2) emissions [2], a set of laws ("Fit for 55" package) has been set to progressively reduce the carbon emissions of various forms of transportation over time [3,4]. This regulatory direction led to a strong push in transport electrification, especially for light-duty applications, with alternative low-lifecycle-CO_2 solutions for applications where full electrification is harder to achieve. The latter group includes heavy-duty vehicles, marine transport, and aviation. Indeed, it is generally acknowledged that the fastest way to achieve carbon neutrality in the transportation sector is a multifaceted approach, given the diversity of applications and short-term targets [5].

Focusing on the reciprocating internal combustion engine (ICE), which is the most adopted technology to power land and maritime transport [6–8], scientific research has increasingly turned to alternative fuels, particularly e-fuels and bio-based fuels. These options offer a

Abbreviations: AMR, Adaptive mesh refinement; aSOC, After the start of combustion; aSOI, After start of injection; CDC, Conventional diesel combustion; CFD, Computational fluid dynamics; CI, Compression-ignition; CRC, Coordinating Research Council; DFI, Ducted fuel injection; DT, Dwell time; DT_{pilot}, Dwell time between pilot and main injection; DT_{post}, Dwell time between main and post injection; ECN, Engine Combustion Network; EGR, Exhaust gas recirculation; EOI, End of injection; FSI, Free spray injection; GHG, Greenhouse gas; HRR, Heat release rate; ICE, Internal combustion engine; ID, Ignition delay; IMEPg, gross indicated mean effective pressure; ISNOx, Indicated specific NOx; ISSoot, Indicated specific soot; LES, Large eddy simulation; LOL, Lift-off length; $m_{f,pilot\%}$, Percentage of the total mass injected in the pilot injection; $m_{f,post\%}$, Percentage of the total mass injected in the post injection; MI, Multi-injection; NL, Natural luminosity; NOx, Nitrogen oxides; SCORE, Sandia compression-ignition optical research engine; SOC, Start of combustion; SOI, Start of injection.

* Corresponding author.
E-mail address: cristiano.segatori@polito.it (C. Segatori).

https://doi.org/10.1016/j.fuproc.2026.108602
Received 18 June 2026; Received in revised form 15 August 2026; Accepted 21 September 2026
Available online 25 September 2026
0378-3820/© 2026 The Authors. Published by Elsevier B.V. This is an open access article under the CC BY license (http://creativecommons.org/licenses/by/4.0/).

practical pathway to lower net CO_2 emissions while remaining compatible with existing ICEs. Considering compression-ignition (CI) engines, which are particularly relevant for heavy-duty applications [9–11], a promising approach to reducing their environmental impact is the coupling of low-lifecycle-CO_2 fuels with Ducted Fuel Injection (DFI) technology [12,13]. The core concept of DFI is to improve air–fuel mixing prior to the lift-off length (LOL) by injecting the fuel through small ducts placed inside the combustion chamber at a specific distance from each injector nozzle hole. DFI promotes improved air–fuel mixing through, first, enhanced air entrainment at the duct inlet due to a suction effect; second, enhanced turbulent mixing due to high velocity gradients; and third, increased LOL [14,15]. These phenomena contribute to a strong reduction in the equivalence ratio at the LOL, thus lowering soot formation [16]. Moreover, the reduction in residence time for soot formation between the LOL and the diffusion flame might also play a role in the DFI-related soot emissions reduction [17]. DFI can also be successfully employed in conjunction with low-lifecycle-CO_2 fuels, being synergic with oxygenated blends (e.g., curtailing soot by two orders of magnitude: one due to DFI and an additional one due to fuel oxygenation) [18,19].

Despite these promising results, the literature has also pointed out the importance of optimizing the combustion system design and the engine calibration for DFI. Various phenomena such as hindered soot oxidation, re-entrainment phenomena, and/or the occurrence of in-duct combustion can limit DFI soot mitigation performance [20–22].

To accelerate the development and commercialization of DFI on production CI engines, a team was formed under the auspices of the Coordinating Research Council (CRC) [23]. This consortium, involving approximately two dozen industrial and research partners, implemented DFI in a heavy-duty multi-cylinder CI engine with production-viable hardware. Project results have been reported in [24]. In this work, the multi-cylinder engine was equipped with DFI and tested using both conventional diesel fuel and lower lifecycle CO_2 fuels. Promising results were achieved, particularly in terms of soot (87%) and NOx (42%) reductions on average over an industry-standard test cycle compared to the production engine calibration when combining DFI with a 50/50 blend of biodiesel and renewable diesel.

Although existing studies reported promising results that underscore the potential of this technology, important research gaps and unresolved challenges remain. A key research gap concerns the interaction between DFI and multi-injection (MI) strategies. With FSI, particularly in light-duty applications, pilot injections are typically adopted for reducing NOx and combustion noise [25–28], while post injections are used for mitigating soot emissions [29]. Piano et al. [22] conducted a numerical analysis investigating the retrofitting of DFI onto an existing light-duty diesel engine. At partial load, an MI strategy optimized for FSI operation was used, composed of two small pilots, one main injection, and one post injection. Despite reduced soot formation, DFI showed higher engine-out soot emissions than FSI, due to weaker soot oxidation. Nevertheless, when the post-injection was removed and the main injection duration was correspondingly increased, the DFI configuration achieved lower engine-out soot emissions than FSI under the same injection pattern.

Liu et al. [30], using the Sandia Compression-ignition Optical Research Engine (SCORE), numerically analyzed the impact of pilot injections on DFI operation. A pilot injection calibration, in terms of start of injection (SOI) and energy share, that improves indicated thermal efficiency without significantly affecting soot and NOx emissions was identified. When Exhaust Gas Recirculation (EGR) was applied, the pilot injection scheme resulted in reduced NOx emissions, although at the expense of increased soot, thus showing trends commonly observed when operating in conventional diesel combustion (CDC) mode.

An improved phenomenological understanding regarding the impact of pilot injections on DFI performance was provided in [31,32]. Wang et al. [31] experimentally observed a faster penetration of the second spray relative to the first for split injections in a constant-volume chamber. In DFI, this behavior was mainly attributed to the reduced gas resistance during the early stage of the second injection, as ambient gas continuously enters the duct throughout the dwell period. Godbold et al. [32] conducted an experimental and numerical campaign at diesel relevant conditions, comparing the spray evolution and combustion behavior resulting from standalone main and pilot-main injection strategies, for both FSI and DFI. The pilot injection was shown to only slightly reduce ignition delay and premixed burn intensity for DFI, reaching levels similar to FSI without a pilot injection. This behavior was associated with an almost identical initial LOL between standalone main and pilot-main injections for DFI, despite the significant reduction observed for FSI with a pilot. This unaffected LOL, combined with the faster and leaner spray tips observed for the pilot-main strategies (both FSI and DFI), corresponded with a significant reduction in soot natural luminosity levels during the transient phase of combustion for DFI coupled with pilot injections. This reduction was not observed for FSI with pilot. All these findings highlight the need for a deeper understanding of the interaction between MI strategies and DFI, due to the different combustion dynamics of FSI approaches.

Considering the above, the aim of the present work is to examine MI strategies with DFI via 3D computational fluid dynamics (CFD) engine simulations. A previously developed and validated (under both FSI and DFI [33]) optical engine model was exploited to analyze the impact of pilot and post injections on DFI performance, supported by optical data from a test vessel experimental campaign. Parametric sweeps were performed on the injected mass during the pilot or post injection and the hydraulic dwell time between the injection event and the corresponding main injection. The analysis focuses on soot and NOx emissions, as well as on the in-cylinder combustion process evolution, with the final goal of identifying the key phenomena characterizing DFI combustion when combined with MI strategies, highlighting differences relative to FSI.

2. Methodology

2.1. Experimental setup: Engine test case

The engine model employed in this study is based on the SCORE, a 1.72-l single-cylinder optical research engine with 125-mm bore and 140-mm stroke. Further details on the engine specifications can be found in [16,34]. Concerning the operating conditions, a detailed description of the experimental campaign is reported in [19]. Among the available data, the present work considers the medium load case (i.e., 10 bar gross indicated mean effective pressure ($IMEP_g$) at 1200 rpm) featuring 16% O_2 level, for both FSI and DFI configurations. This mid-load point is representative of a typical operating condition for heavy-duty engines and, according to previous studies, the selected 16% intake O_2 concentration corresponds to the upper dilution limit for FSI before a significant increase in engine-out soot emissions occurs, whereas even higher dilution levels may be achievable with DFI [19].

Regarding the DFI configuration, the adopted duct design corresponds to the D3L12G3δ setup (Fig. 1), featuring a four-duct module with a 3.0 mm internal diameter (D), 12.0 mm length (L), and 3.0 mm gap (G) between the injector orifice outlet and the duct inlet plane. These dimensions were identified as suitable for reducing soot emissions while preserving fuel conversion efficiency with the injector employed in the present study [35]. Among the four nozzle geometries investigated in [36], the δ geometry, featuring a rounded inlet and a tapered outlet, resulted in the lowest soot formation.

A summary of the engine geometric and operating parameters is reported in Table 1.

2.2. Numerical setup

In [33], a high-fidelity 3D-CFD model for the SCORE was developed using the commercially available software CONVERGE CFD [37]. Particularly, the model was validated for both FSI and DFI

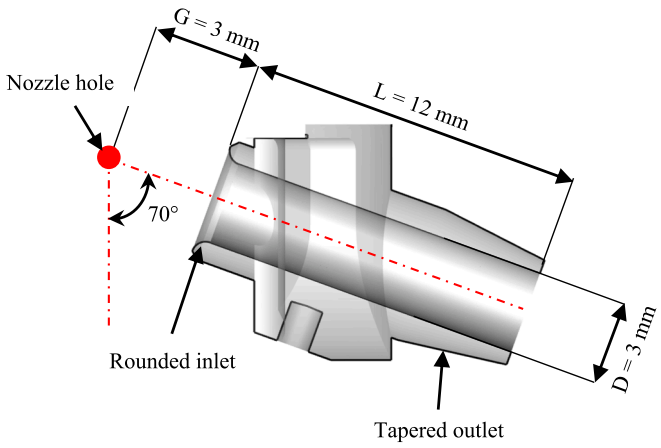


Fig. 1. Sketch of the D3L12G3δ duct design.

Table 1
Summary of engine details, operating conditions, injection system, and duct configuration.

Displacement	1.72 L
Bore	125 mm
Stroke	140 mm
Squish height	1.5 mm
Geometric compression ratio	12.5:1
Effective compression ratio	11.9:1
Engine speed	1200 rpm
Engine load (IMEPg)	10 bar
Oxygen concentration	16 mol%
Injector position	Central-mounted
Injection pressure	180 MPa
Nozzle hole diameter	4 holes × 0.175 mm
Spray umbrella angle	140°
Duct geometry (if present)	D3L12G3δ

configurations, for different oxygen concentrations, in terms of both combustion behavior - including pressure and burn rate traces and LOL - as well as engine-out soot and NOx emissions. Additionally, to validate the predicted soot formation and oxidation processes, a virtual natural luminosity (NL), derived from CFD outputs through a dedicated methodology, was compared with experimental soot NL optical images. The main characteristics of the numerical setup are summarized in Table 2; for further information about the model development process and validation, please refer to [33].

Table 2
3D-CFD setup summary for engine simulations.

Simulation approach	Engine sector combustion simulations
Simulation initialization	Full-cylinder cold-flow simulation
Simulation window	From IVC (−153 CA deg aTDCf) to EVO (123 CA deg aTDCf)
Base grid size	1 mm
Grid refinement technique	Local embedding and Adaptive Mesh Refinement (AMR) [37]
Minimum grid size (global domain)	0.125 mm
Minimum grid size for y+ control (duct wall)	0.0625 mm
Turbulence model	RANS Standard k-ε [38] (with round jet correction [39])
Heat Transfer model	O′ Rourke and Amsden model [40]
Thermal boundary condition	Standard wall functions with wall temperature values from [30]
Spray model	Validated against ECN "Spray D" data [41]
Combustion model	SAGE detailed chemistry solver (equipped by the Skeletal Zeuch combustion mechanism [42])
NOx model	Extended Zel'dovich mechanism [43]
Soot formation/oxidation	Particulate Mimic model [44]

3. DFI and multi-injection strategies

This work aims to investigate the effects of MI strategies in conjunction with DFI technology. To this end, the developed engine model was employed to study the individual impacts of pilot injections and post injections on DFI performance under CI engine conditions. A parametric analysis was conducted, sweeping hydraulic dwell time (DT) and mass share ($m_{f,\%}$) in each injection event. The nomenclature of each parameter is defined in Fig. 2, illustrating both an exemplary multi-injection profile and the original single-injection profile.

The fuel mass share in each injection event was adjusted to keep the total injected mass constant and equal to the single-injection case. The resulting load variations associated with the pilot and post-injection calibrations were found to remain within an acceptable range; in all cases, they were below 1.2%.

3.1. The impact of pilot injection on DFI performance

The influence of pilot injections on DFI performance was assessed by varying both the hydraulic dwell time DT_{pilot} and the fuel mass share $m_{f,\%}$ between the pilot and main injections. The tested operating conditions fall within the conventional CI engine calibration range and are summarized in Table 3.

Fig. 3 shows the percentage variation in indicated specific soot (ISSoot) and NOx (ISNOx) emissions relative to the standalone main baseline for both FSI and DFI configurations.

Considering soot emissions, the results for both injection strategies indicate that moving toward lower DT_{pilot} values while increasing $m_{f,pilot\%}$ results in lower emission levels, although the influence of $m_{f,pilot\%}$ at low DT_{pilot} values is more pronounced for FSI. Overall, when comparing the ISSoot values obtained in both configurations, FSI exhibits greater variability, thus suggesting the lower sensitivity of DFI combustion to the introduction of a pilot injection compared to FSI.

As expected, NOx emissions exhibit opposite trends, with a general reduction when DT_{pilot} is increased and $m_{f,pilot\%}$ is reduced for both FSI and DFI configurations. Consequently, the most substantial reduction in NOx emissions compared to the single-injection baselines is observed for the case with a 15 CA deg DT_{pilot} and 5% $m_{f,pilot\%}$ in both configurations. Consistent with the behavior observed for soot, FSI also exhibits greater sensitivity than DFI to pilot injection calibration in terms of NOx.

Fig. 4 shows how the DFI configuration performs relative to the FSI configuration at equal pilot injection calibration. Specifically, Δ_{DFI} is defined as the percentage change in ISSoot or ISNOx induced by DFI

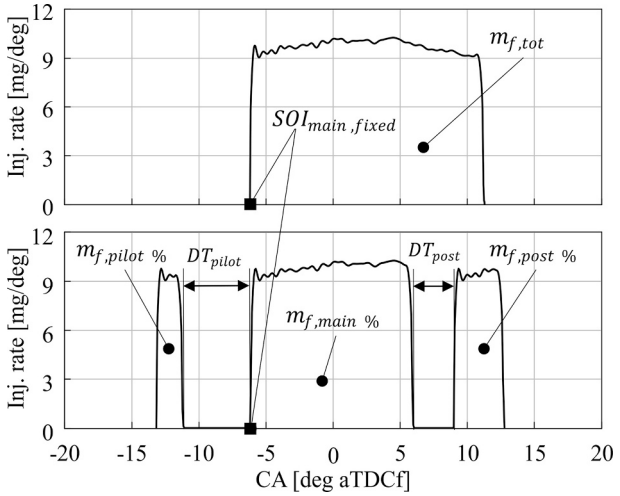


Fig. 2. Schematic illustration of the original single-injection profile (top) and derived multi-injection pattern (bottom), covering both pilot-main and main-post injection configurations.

Table 3
Test matrix for the pilot-injection analysis. Please refer to Fig. 2 for nomenclature.

DT_{pilot} [CA deg]	$m_{f,pilot\%}$ [%]	$m_{f,main\%}$ [%]	DT_{post} [CA deg]	$m_{f,post\%}$ [%]
5	5	95	\	0
5	10	90	\	0
10	5	95	\	0
10	10	90	\	0
15	5	95	\	0
15	10	90	\	0

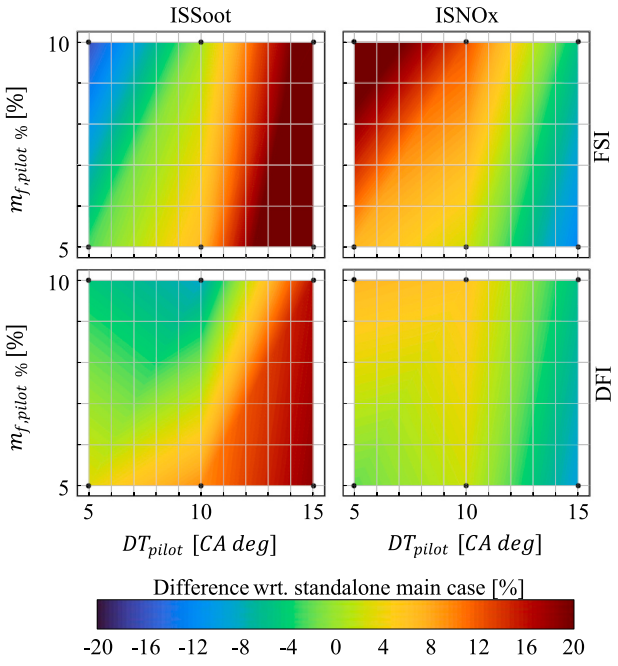


Fig. 3. Percentage difference between the multi-injection case (pilot-main injection) and standalone main case as a function of DT_{pilot} and $m_{f,pilot\%}$, for indicated specific soot (left) and NOx (right) emissions, for both FSI (top) and DFI (bottom) configurations.

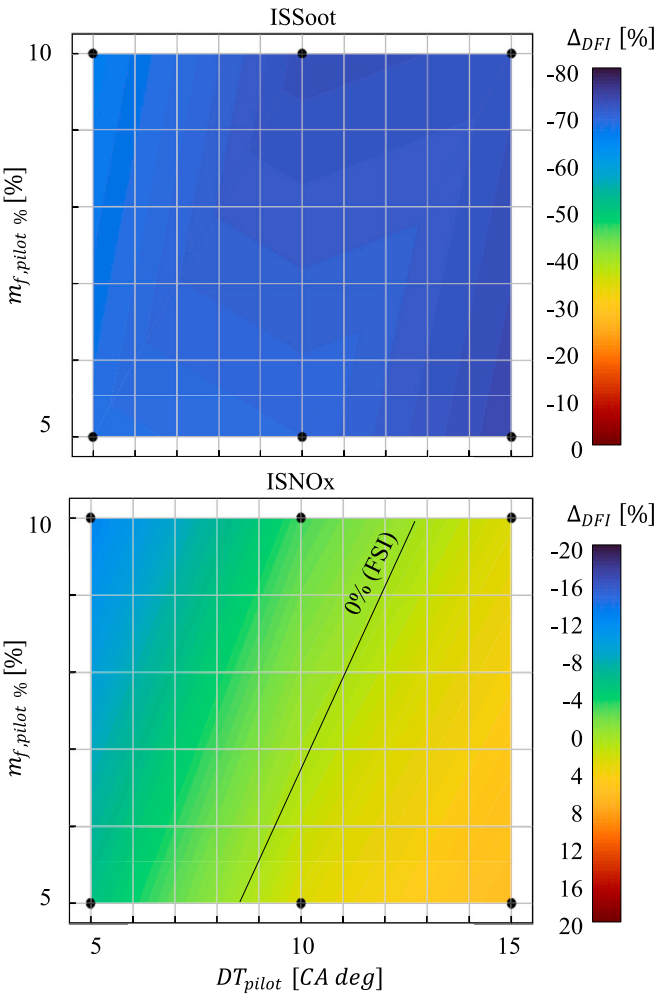


Fig. 4. Percentage difference between DFI and FSI configurations for the MI case (pilot-main injection) as a function of DT_{pilot} and $m_{f,pilot\%}$, for indicated specific soot (top) and NOx (bottom) emissions.

relative to FSI. The first notable result is that soot emissions are consistently lower (approx. -70%) for the DFI configuration across all tested conditions. This confirms that DFI remains effective in its main purpose, even when a pilot injection is added to a main injection. Furthermore, analyzing NOx emissions, while DFI typically shows slightly higher NOx than FSI with the standalone main strategy [45,46], this trend can reverse under certain pilot injection calibrations. In particular, as DT_{pilot} is decreased and $m_{f,pilot\%}$ is increased, the relative performance of DFI in terms of NOx emissions improves, thus defining a region in the contour plot with a NOx emission advantage compared to FSI. In other words, DFI exhibits a different physical response to the introduction of the pilot injection, resulting in improved performance compared to FSI in terms of NOx emissions for certain pilot calibrations, while maintaining a large reduction in soot.

The condition with 10% $m_{f,pilot\%}$ and 5 CA deg DT_{pilot} is particularly relevant, as it features the largest NOx reduction for DFI compared to FSI. Consequently, a more detailed analysis of the combustion behavior for this condition will be presented in the following section, comparing FSI and DFI configurations.

Fig. 5 shows the pressure traces and heat release rate (HRR) profiles for both configurations, together with the standalone main results as a reference. The introduction of a pilot injection produces markedly different effects depending on the injection strategy. Indeed, following a similar combustion behavior during the pilot phase, where FSI shows a slightly shorter ignition delay (ID) than DFI, the FSI configuration experiences a significant reduction in the ID of the main injection, while an appreciable ID is retained for the DFI. This leads to a significant reduction in the premixed combustion intensity for FSI, whereas only a slight decrease is observed for DFI, compared to the standalone main case. Both FSI and DFI feature a more intense mixing-controlled phase when pilot injection is used.

These results are consistent with previous experimental findings under test vessel conditions [32], and a quantitative comparison in terms of ID and premixed burn intensity values is reported in Fig. 6, given the comparable operating conditions. In both datasets, the pilot-main strategy leads to a significant ID reduction for FSI, while the reduction is less pronounced for DFI. This trend is reflected in the premixed burn intensity, with FSI showing a strong decrease with pilot-main injection, while DFI retains a substantial premixed phase, with values closer to those of FSI in the standalone main case.

To investigate the origin of these differences, Fig. 7 presents the local HRR distribution on the vertical plane of the engine sector containing the injector and spray axes for both FSI and DFI in the pilot-main case. Consistent with test-vessel experimental observations, DFI exhibits a longer ID than FSI, also for pilot combustion. In the FSI case, the HRR signal is highly visible at 2.9 CA deg before SOI_{main}, highlighting pilot combustion flame, whereas in DFI it is not visible. At 2 CA deg before SOI_{main}, the FSI pilot flame develops closer to the injector region due to combustion recession. In contrast, in the DFI configuration, the pilot combustion flame is located closer to the piston wall, without a

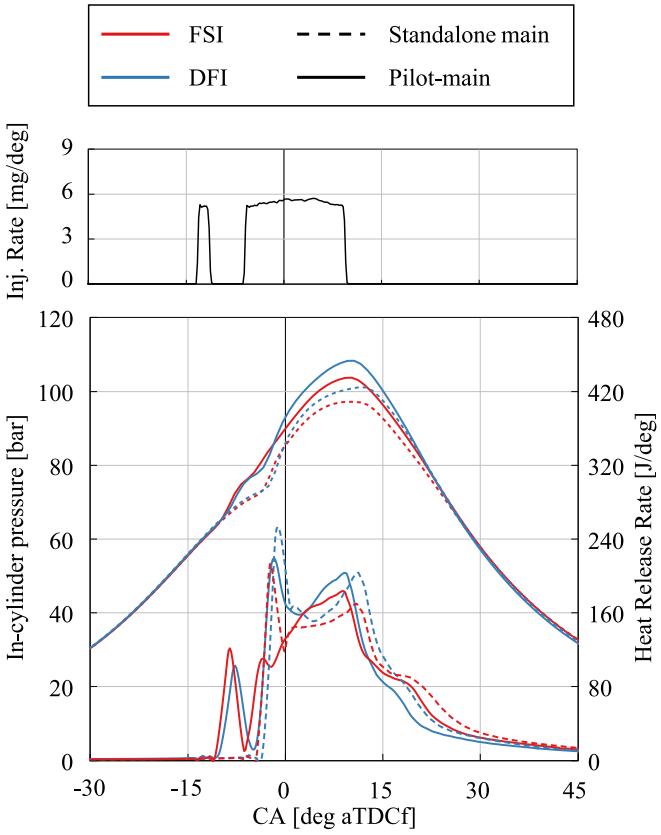


Fig. 5. Injection rate (top), in-cylinder pressure and heat release rate (bottom) for both FSI (red) and DFI (blue). Standalone main case shown as dashed lines, pilot-main case (DT_{pilot} = 5 CA deg and $m_{f,pilot}$ = 10% $m_{f,tot}$) as solid lines. (For interpretation of the references to colour in this figure legend, the reader is referred to the web version of this article.)

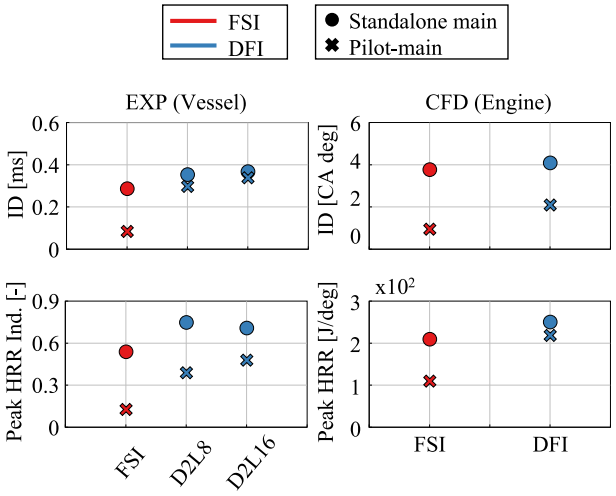


Fig. 6. Experimental vessel-derived data (left) and engine simulation results (right) for ignition delay (ID, top) and peak heat release rate (HRR) of the premixed burn phase (bottom) of the main injection. FSI configuration results are shown in red, DFI in blue. Standalone main injection strategy is represented by circle markers, while pilot-main injection scheme is indicated by X markers. Pilot-main scheme: DT_{pilot}= 0.8 ms and $m_{f,pilot}$= 2.5 mg for vessel, DT_{pilot}= 0.7 ms (i.e., 5 CA deg) and $m_{f,pilot}$= 10% (i.e., 2.3 mg) for engine. Details on the experimental campaign in [32]. (For interpretation of the references to colour in this figure legend, the reader is referred to the web version of this article.)

significant combustion recession. This different positioning of the pilot flame and of the resulting hot combustion products leads to earlier ignition of the main injection in the FSI case, which becomes visible at 0.8 CA deg $aSOI_{main}$, as indicated by the HRR turning positive along the isoline tracking the fuel spray. In contrast, for DFI, ignition occurs only around 2.3 CA deg $aSOI_{main}$, when the main jet has travelled for a longer distance and interacts with the peripheral hot-products region generated by the pilot combustion.

A similar behavior was also observed in vessel experiments, as shown in Fig. 8, which shows the OH* chemiluminescence (an indicator of high-temperature heat release) at four time instants for FSI and DFI with a pilot-main injection scheme. Moving from top to bottom, several common phenomena can be observed. At 0.2 ms before SOI_{main}, combustion recession is observable for FSI, whereas no combustion recession is observed for DFI. This leads to the presence of radicals and hot products near the injector at SOI_{main} for FSI, but not for DFI. As a result, looking at a time instant just after SOC_{main}, the FSI main flame ignites close to the injector as evidenced by the higher luminosity in the near injector region compared to the previous time instant (i.e., SOI_{main}). On the other hand, the main injection penetrates farther before igniting for DFI, thus resulting in a LOL location similar to the standalone main case [32]. This allows DFI to partially preserve the ID and the premixed burn intensity. Circle markers help identify the ignition location of the main injection in both the FSI and DFI configurations. Finally, at 0.24 ms aSOI, the flame stabilizes with a longer LOL for DFI than for FSI, similarly to the standalone main case.

To quantitatively compare these behaviors, Fig. 9 represents the time evolution of LOL for both test-vessel experiments and engine simulations, comparing the standalone main and pilot-main schemes for both FSI and DFI. In the experimental results (Fig. 9, top), combustion recession is clearly observed in the FSI configuration at the pilot EOI. Specifically, LOL decreases significantly from approximately 15 to 3 mm before the SOI_{main}. This recession promotes rapid ignition of the main spray (identifiable as the time instant at which the LOL curve drops sharply $aSOI_{main}$). Thus, the initial LOL of the main combustion is reduced in the pilot-main scheme relative to the standalone main scheme. In contrast, the combustion recession is less significant for the DFI case, likely due to the leaner mixture at the spray tail and its higher axial velocity (see fig. 11 of [32]), showing a LOL shortening of only 2 mm at EOI_{pilot}. As a consequence, ID is partially preserved (Fig. 6) and the initial LOL of the main combustion remains unchanged when the pilot injection is used.

Similar trends are observable in the engine simulations (Fig. 9, bottom). In FSI, the LOL after the EOI_{pilot} exhibits a stronger recession than DFI, albeit this difference is relatively lower than experiments. Longer IDs, interaction between spray and walls, and different turbulent conditions could explain this discrepancy. The stronger pilot recession for FSI causes a reduced ID of the main injection (Fig. 6), thus shortening its initial LOL, as in experiments. Despite being smaller than that for FSI, an initial LOL reduction is also present for the DFI case, in contrast to the experimental results. This discrepancy could be attributed to the higher temperature and pressure values encountered by the main injection when preceded by a pilot in engine simulations, whereas the conditions between standalone main and pilot-main schemes are much closer in the experimental vessel campaign. Finally, as the injection progresses, the LOL of the pilot-main case tends to approach the LOL values observed for the standalone main injection, in both experiments and simulations.

In conclusion, when low DT_{pilot} and high $m_{f,pilot\%}$ values are employed, the numerical results highlight a strong interaction between pilot and main injection for FSI, and a reduced interaction for DFI. These observations are supported by experimental evidence under test vessel conditions. For FSI, the flame evolution promotes higher NOx formation, likely due to the increase in local temperatures caused by the ignition of the main spray in the still high-temperature products of the pilot flame. In contrast, for DFI, the delayed interaction between the main spray and the pilot flame allows the pilot combustion products to cool further before the ignition of the main spray, thereby reducing the local ther-

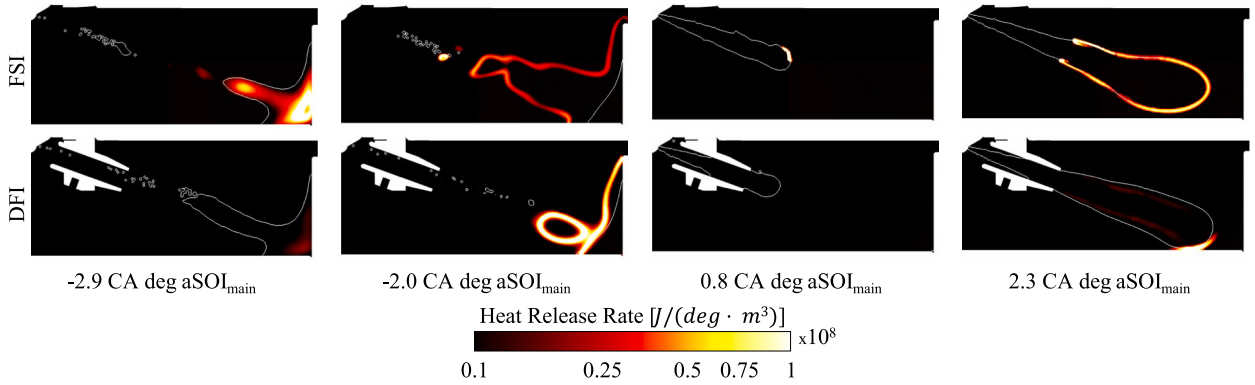


Fig. 7. Heat release rate (HRR) distribution shown on a logarithmic scale in a vertical plane including the injector and spray axes in the pilot-main scheme with $DT_{pilot} = 5$ CA deg and $m_{f,pilot\%} = 10\%$., for both FSI (top) and DFI (bottom) configurations at different time instants (−2.9 deg $aSOI_{main}$, −2.0 deg $aSOI_{main}$, 0.8 deg $aSOI_{main}$ and 2.3 deg $aSOI_{main}$). The isoline representing fuel injection corresponds to an overall equivalence ratio of 1.

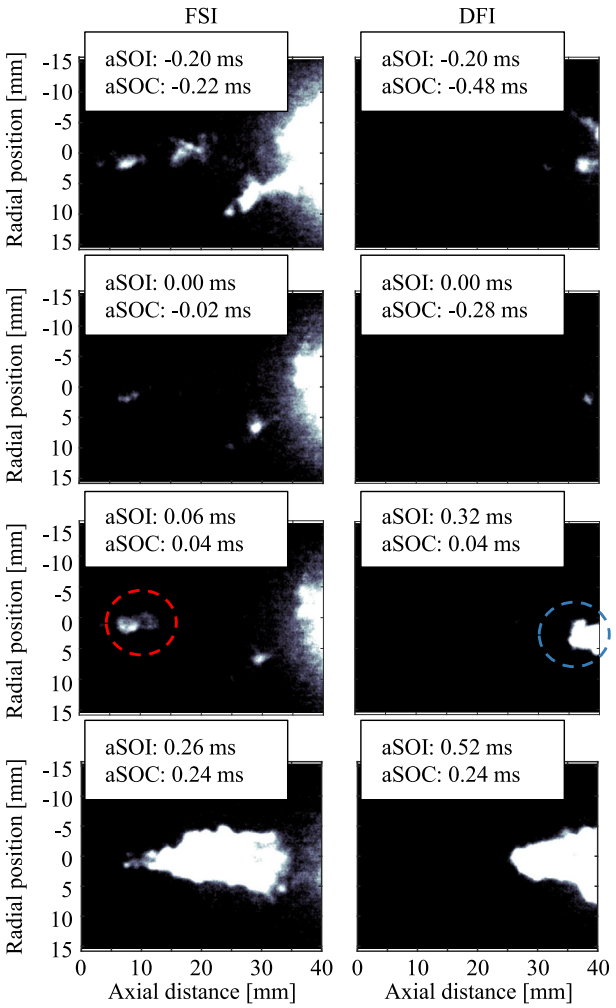


Fig. 8. Experimental OH* chemiluminescence images for (left) FSI and (right) DFI (D2L8 configuration) captured at four time instants for the pilot-main injection scheme: (from top to bottom) combustion recession of the pilot combustion at 0.2 ms before SOI$_{main}$; SOI$_{main}$; SOC$_{main}$; developed flame at 0.24 ms aSOC$_{main}$. Circle markers indicate the ignition location of the main injection.

modynamic conditions that favour NOx formation compared to FSI. While this interpretation appears physically plausible, further analyses are required to validate it and are beyond the scope of the present work.

Pilot injection strategies are typically used for combustion noise mitigation, by reducing the premixed burn intensity. DFI with a single-injection strategy has been shown experimentally to increase the combustion noise due to the more intense premixed combustion than FSI [45]. Therefore, it becomes important to understand if pilot injection can be effectively used in conjunction with DFI for noise mitigation. Fig. 10 reports the values of maximum rate of pressure rise - which is a primary indicator for combustion noise [47] - associated with the tested pilot calibrations on a normalized ISSoot-ISNOx diagram, for both FSI and DFI configurations. Standalone main values are also reported for reference.

In the standalone main case, DFI exhibits a significantly higher maximum pressure rise rate than FSI, while it achieves a strong reduction in soot and slightly higher NOx emissions. When a pilot injection is introduced, the two configurations respond differently. FSI shows a consistent reduction in maximum pressure rise rate for each pilot injection calibration, with emissions varying in a relatively large range on a typical soot-NOx trade-off path. In contrast, DFI exhibits a less pronounced change in maximum pressure rise rate, but with a flatter soot-NOx trade-off and a narrower emissions range in response to pilot injection. A significant reduction in maximum pressure rise rate is achieved only for the 10% $m_{f,pilot\%}$ and 5 CA deg DT_{pilot} case, achieving a level like that of FSI in the standalone main configuration. This is in line with previous findings, particularly with the lower sensitivity of the DFI mode to the introduction of a pilot injection, which begins to play a significant role only when the interaction between the main injection and the pilot flame becomes stronger, that is, under conditions of lower DT_{pilot} values times combined with higher $m_{f,pilot\%}$ values. As a consequence, a dedicated pilot injection calibration will likely be needed for DFI if combustion noise reduction is a priority.

3.2. The impact of post injection on DFI performance

As performed for the pilot-injection investigation, the influence of post injection on DFI performance under engine conditions was assessed by varying both the hydraulic dwell time DT_{post} and the fuel mass share $m_{f,post\%}$ between main and post injections. The tested operating conditions fall within the conventional CI engine calibration range and are summarized in Table 4.

In Fig. 11, the percentage variation in ISSoot and ISNOx emissions relative to the standalone main case are presented for both configurations.

Regarding soot emissions, a significant reduction is achieved in both FSI and DFI configurations when a post-injection is introduced, confirming the effectiveness of this strategy in mitigating engine-out soot emissions [29]. Depending on the post injection calibration, the soot reduction relative to the standalone main case ranges between approximately 20% and 60%, for both configurations.

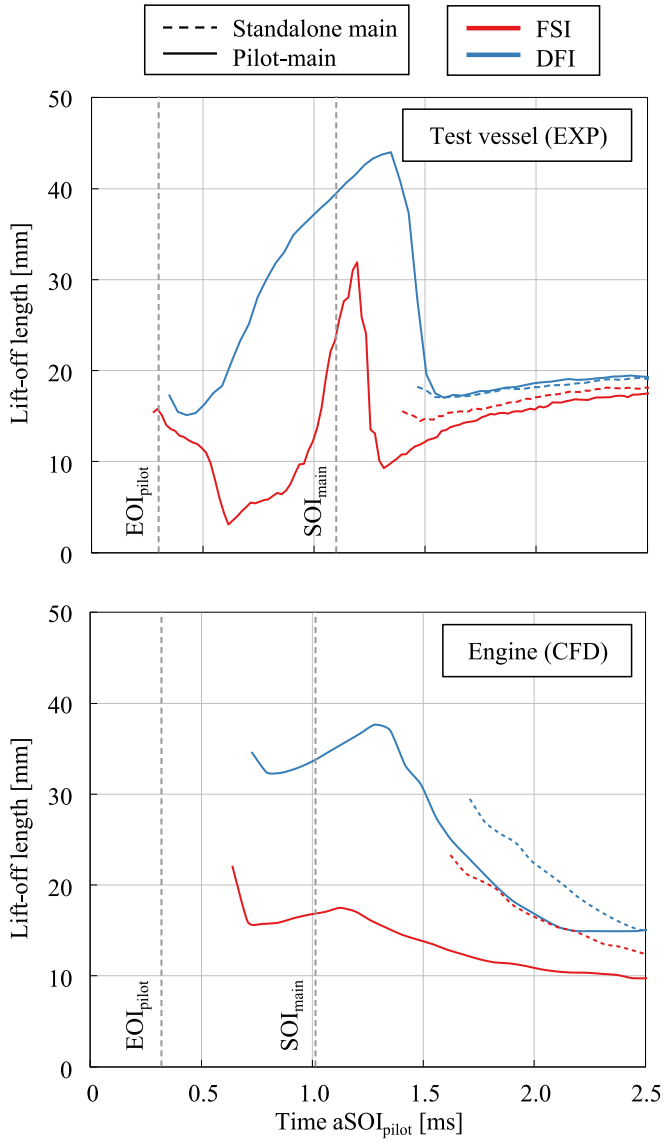


Fig. 9. Time evolution of lift-off length from vessel experiments (top) and engine simulations (bottom) for FSI (red) and DFI (blue) configurations. Solid lines represent pilot injection cases, while dashed lines correspond to standalone main cases. Pilot-main scheme: DT_{pilot} = 0.7 ms (i.e., 5 CA deg) and $m_{f,pilot\%}$ = 10% (i.e., 2.3 mg) for engine, DT_{pilot} = 0.8 ms and $m_{f,pilot}$ = 2.5 mg for vessel. (For interpretation of the references to colour in this figure legend, the reader is referred to the web version of this article.)

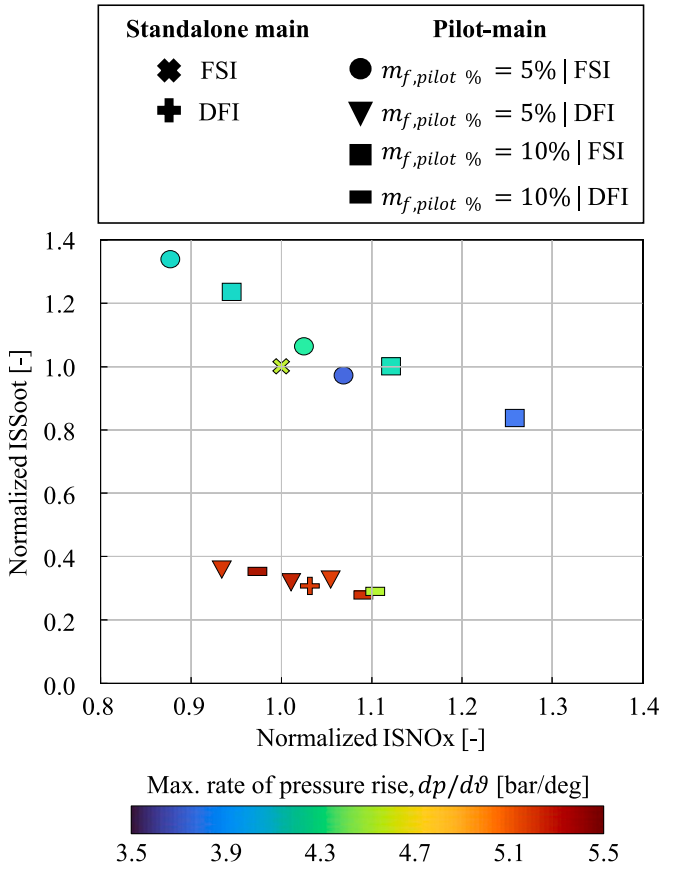


Fig. 10. Scatter plot of maximum rate of pressure rise, used as a combustion noise indicator, on a normalized indicated specific soot-NO_x diagram. Standalone main cases are shown with X markers for FSI and cross markers for DFI configurations. Multiple injection cases are represented with circles for FSI and $m_{f,pilot\%}$= 5%, triangle markers for DFI and $m_{f,pilot\%}$ = 5%, square markers for FSI and $m_{f,pilot\%}$ = 10%, and rectangular markers for DFI and $m_{f,pilot\%}$ = 10%.

In the FSI configuration, the observed soot reduction depends primarily on $m_{f,post\%}$, with DT_{post} having little influence across the tested points. In contrast, the DFI configuration exhibits a different behavior: while soot emissions at shorter dwell times (i.e., below 6 CA deg) mainly depend on $m_{f,post\%}$, a clear sensitivity to DT_{post} emerges at longer dwell times. This divergence in behavior between FSI and DFI suggests, as for pilot injection, a different interaction between the main combustion and post-injection, which becomes more evident as the DT_{post} increases, as addressed later in the text.

Concerning NOx emissions, a modest reduction is generally observed across most operating points, with DFI configuration showing higher reduction levels. The only exception is the FSI case with 20% $m_{f,post\%}$ and 3 CA deg DT_{post}, where a slight increase in NOx emissions is recorded. Nevertheless, the magnitude of NOx reduction is significantly lower than that observed for soot, for which the post-injection strategy is conceived. Specifically, in the FSI configuration, NOx emissions tend to increase as DT_{post} decreases. The DFI configuration features a similar general trend, though less pronounced. The observed NOx reduction at higher dwell times may be attributed to a decrease in peak flame temperature. Indeed, as DT_{post} increases, first, the main combustion flame has more time to cool down before the post-injection occurs, and second, a portion of the combustion is moved later in the expansion stroke. Consequently, the post-injection is introduced into a lower-temperature environment compared to a continuous single-injection event, reducing flame temperature and, thus, thermal NO formation.

Table 4
Test matrix for the post-injection analysis. Please refer to Fig. 2 for nomenclature.

DT_{pilot} [CA deg]	$m_{f,pilot\%}$ [%]	$m_{f,main\%}$ [%]	DT_{post} [CA deg]	$m_{f,post\%}$ [%]
\	0	90	3	10
\	0	80	3	20
\	0	90	6	10
\	0	80	6	20
\	0	90	9	10
\	0	80	9	20
\	0	90	12	10
\	0	80	12	20

As done for the pilot injection analysis, Fig. 12 reports the percentage difference in soot and NOx emissions between DFI and FSI configurations at equal post injection calibration. Across all tested points, DFI outperforms FSI, yielding lower soot emissions, thus demonstrating the possibility of successfully coupling this technology with post-injection

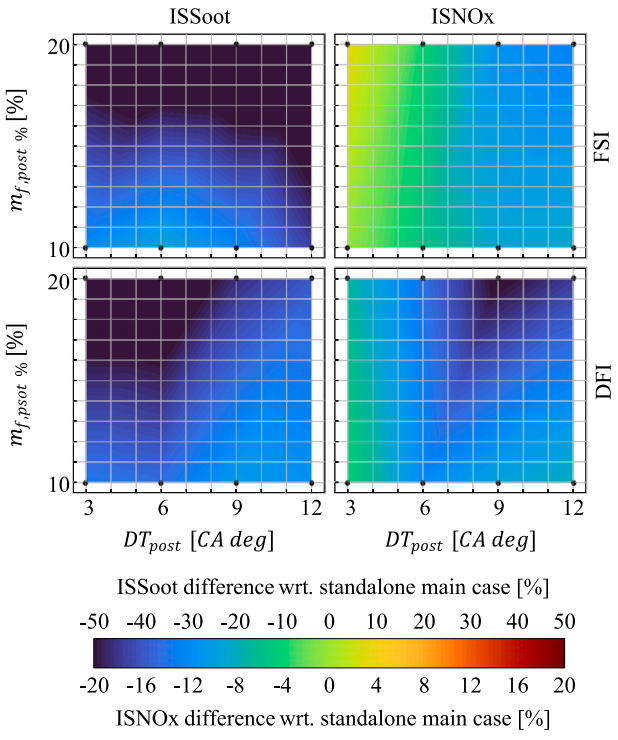


Fig. 11. Percentage difference between the multi-injection case (main-post injection) and standalone main case as a function of DT_{post} and $m_{f.post\%}$, for indicated specific soot (left) and NOx (right) emissions, for both FSI (top) and DFI (bottom) configurations.

strategies. Nevertheless, the magnitude of its advantage over FSI is strongly dependent on the adopted DT_{post}, with $m_{f.post\%}$ becoming more important moving toward higher values of dwell time. Indeed, the soot reduction achieved by DFI relative to FSI ranges from approximately 50% to 75%, compared to a 72% reduction observed for the standalone main baseline. This highlights the importance of proper post-injection calibration to fully exploit the potential of DFI. Moreover, apart from soot, the results demonstrate that the introduction of post injection also can create conditions for reducing NOx emissions with DFI, similarly to the pilot-injection analysis.

To gain deeper insight into the soot formation/oxidation process and the performance worsening of the DFI configuration at higher DT_{post}, Fig. 13 reports the in-cylinder soot mass, normalized with respect to the peak value obtained in the FSI standalone main case, for both FSI and DFI considering three injection strategies: the standalone main case and post-injection cases (20% $m_{f.post\%}$) with 3 CA deg and 12 CA deg DT_{post}.

As shown, in the standalone main case, soot mass initially increases and then decreases once a peak value is reached. This time evolution reflects the balance between soot formation and oxidation rate, with oxidation becoming dominant once the soot mass peak value has been reached. A similar behavior is observed for the post-injection strategy with 3 CA deg DT_{post}, though the peak occurs earlier and reaches a lower value. This lower peak value can be attributed to the jet replenishment effect [48], which suggests that soot formation is dependent on the injection duration. A shorter injection duration limits the time available for the fuel-rich region of the jet to be replenished with fresh fuel, thus reducing the overall soot formation. This effect is still observable in the case with 12 CA deg DT_{post}. Indeed, the initial portion of the soot evolution remains the same between the two post-injection strategies, due to the identical main injection duration leading to the same soot mass peak values, but a divergence becomes evident in the later phase of the engine cycle. In the 12 CA deg DT_{post} case, a significant increase in soot mass appears around 25 CA deg aTDCf, indicating a reversal in the soot formation-oxidation balance, with formation once again exceeding

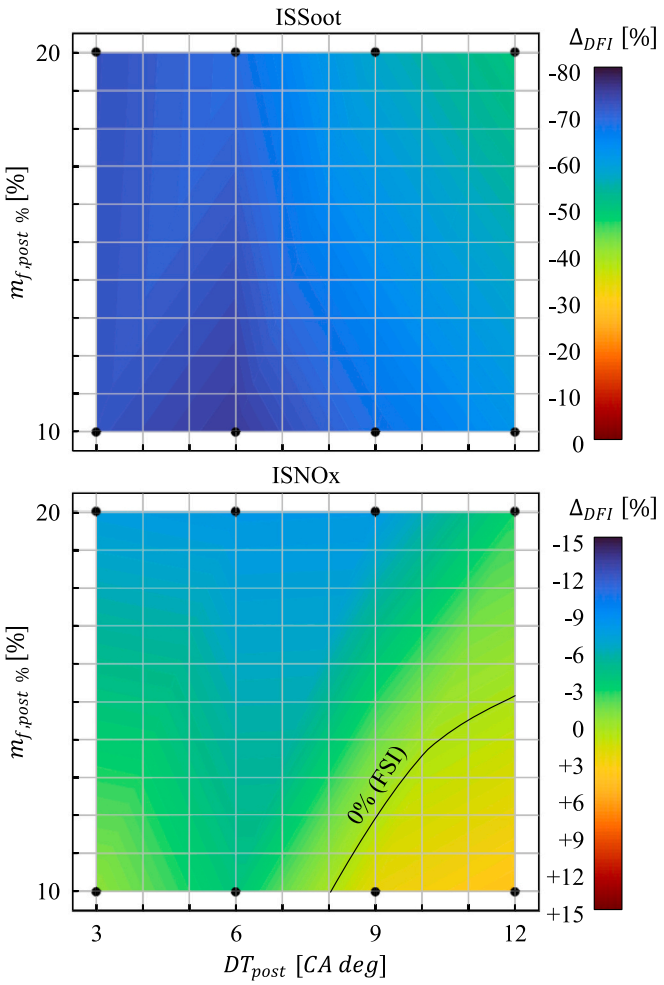


Fig. 12. Percentage difference between DFI and FSI configurations for the MI case (main-post injection) as a function of DT_{post} and $m_{f.post\%}$, for indicated specific soot (top) and NOx (bottom) emissions.

oxidation for a period. Although this late-cycle soot increment is visible in both FSI and DFI configurations, its magnitude differs substantially. In the DFI case, the rise is steeper, even exceeding the soot mass observed at the same time in the standalone main case. Moreover, while the final soot mass for the FSI configuration with 12 CA deg DT_{post} remains lower than the corresponding 3 CA deg case, due to enhanced post-oxidation favored by higher in-cylinder temperatures and mixing, this is not true for DFI. In this case, the benefits of increased mixing and temperature leading to enhanced oxidation are likely outweighed by a higher soot formation rate, thus limiting the post-injection effectiveness.

The observed dependence of soot evolution on the adopted DT_{post}, along with gradual reduction of DFI benefits with respect to FSI mode as DT_{post} is increased, underscores the need for a detailed analysis of the interaction between the main combustion flame and the post-injection event. Fig. 14 illustrates the temperature distributions in a top view of the plane containing the spray axis, at various time instants during the post-injection phase for FSI and DFI configurations featuring 20% $m_{f.post\%}$, with DT_{post} of 3 CA deg and 12 CA deg. For visualization purposes, the single-sector results are mirrored to reconstruct a full-cylinder representation.

Starting from the same temperature distribution at the main EOI, clear differences emerge at the post SOI when comparing the two DT_{post} cases in both configurations. For the case with $DT_{post} = 3$ CA deg, each flame has started to recirculate in the horizontal plane, due to the interaction with adjacent spray flames. In the 12 CA deg case, this recirculation process has progressed further, leading to part of the main

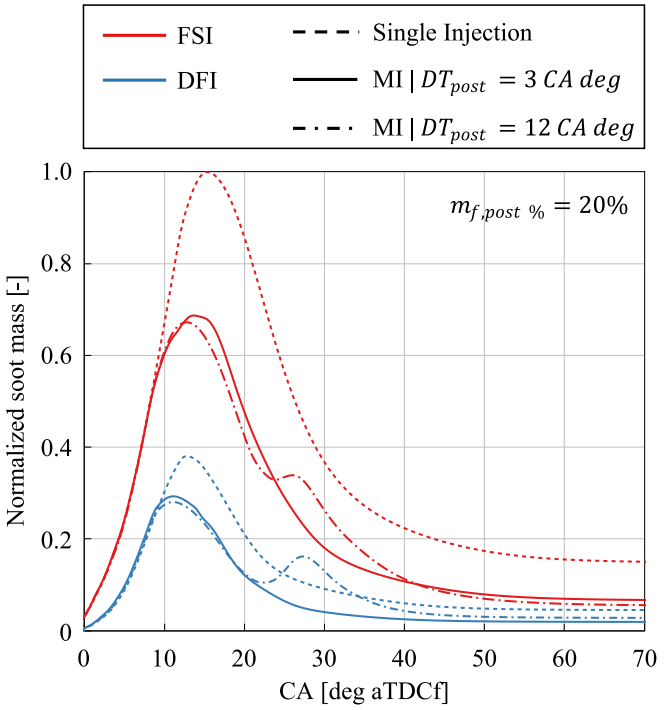


Fig. 13. Normalized soot mass as a function of the crank angle, for both FSI (red) and DFI (blue) for the standalone main case (dashed line) and main-post cases with DT_{post} = 3 CA deg (solid line) and DT_{post} = 12 CA deg dwell time (dash-dot line) and $m_{f,post\%}$ = 20%. (For interpretation of the references to colour in this figure legend, the reader is referred to the web version of this article.)

flame intersecting the spray path. This is even more evident in the DFI configuration, where faster flame penetration further promotes the recirculation process, leading to part of the main flame being upstream of the duct exit (though outside the duct) at SOI_{post}. This results in an almost immediate interaction between the main flame and the post-injection spray, as observed at 1 CA deg $aSOI_{post}$ for both configurations. This early interaction causes prompt ignition and a shortened LOL, thus increasing soot formation related to the post injection, particularly for the DFI configuration, for which benefits from enhanced mixing upstream of the LOL [14,15] are prevented. On the other hand, with a shorter dwell time of 3 CA deg, the post-injection spray interacts with the recirculated main flame later in the injection event, around 3 CA deg $aSOI_{post}$. In this case the post injection ignition is driven by auto-ignition or interaction with the wake of the main flame, especially for FSI due to the stronger combustion recession, similarly to the pilot injection analysis. Therefore, longer LOLs are preserved for both FSI and DFI. This is particularly relevant for the latter, because a longer LOL enables better exploitation of the enhanced mixing downstream of the duct, thus maintaining its advantages relative to FSI.

Moreover, in DFI mode, a longer DT_{post} allows the main flame more time to recirculate close to the duct entrance. This means that the typical pumping effect driven by the spray passing through the duct [14,15] causes the entrainment of hot combustion products rather than fresh air in the duct inlet, leading to ignition of the post-injection spray inside the duct, as evident from 3 CA deg $aSOI_{post}$ to EOI_{post}, for the longer DT_{post} case. This in-duct combustion phenomenon, which is highly detrimental for DFI operation due to a drastic increase in soot formation [12,22,49], is not present for the shorter DT_{post} case, because the main flame has insufficient time to recirculate close to the duct inlet.

To better quantify the influence of DT_{post} on this phenomenon, Fig. 15 presents the mass flow rate of hot combustion products through the duct inlet section during the post injection. Specifically, to ensure that only combustion products were tallied, only species other than air (O_2 and N_2) and fuel vapor (n-C_7H_{16}), and featuring a temperature higher than 1600 K, were considered in the computation. The mass flow rate of hot products entering the duct presents a clear positive dependence on the adopted DT_{post}, because it is related to the amount of time available for main-flame recirculation. In the case with the highest DT_{post} of 12 CA deg, a significant amount of hot combustion products is entrained into the duct; this recirculation diminishes progressively with shorter DT_{post} values, eventually becoming zero for the whole post-injection window in the case with the lowest DT_{post} of 3 CA deg. It is worth noting that not only the mass flow rate values but also the duration over which they are positive is a function of DT_{post}. For instance, the phenomenon affects more than half of the injection duration (approximately 2.5 CA deg) in the 12 CA deg case, but only 1 CA deg of injection in the 6 CA deg case. Because this re-entrainment of hot combustion products causes in-duct combustion, which is directly linked to higher soot formation with DFI, these trends help explain the observations reported in Fig. 12 and Fig. 13. It is noteworthy that the present phenomenological understanding is also likely to play a crucial role when DFI is coupled with single injections featuring very long injection durations. In that case, the re-entrainment of hot products at the duct inlet during the injection, due to the sufficient time for main flame recirculation, can cause a sudden increase in soot formation. These are the so-called “late-cycle flare-ups” experimentally observed in [34] and explainable with the present CFD analysis. In conclusion, the observed differences between DFI and FSI combustion using the post injection strategy highlight the necessity for a dedicated calibration for DFI (e.g., shorter DT_{post} than might be optimal for FSI), in order to fully exploit the soot reduction potential offered by this technology. As a matter of fact, the critical dwell time for in-duct hot-product re-entrainment is expected to depend on injection calibration (e.g., injection pressure, SOI, DOI), in-cylinder ambient conditions, and engine geometry (e.g., duct length and bowl design).

4. Conclusions

This work presented a numerical investigation of the interaction between Ducted Fuel Injection (DFI) and Multi-Injection (MI) strategies. The analysis was conducted using a validated 3D-CFD model based on the Sandia Compression-ignition Optical Research Engine (SCORE), under a representative operating condition of 10 bar IMEPg at 1200 rpm, and 16% oxygen concentration. The numerical model reproduced the main experimental observations associated with DFI coupled with pilot injection.

The engine model was employed to assess the impact of introducing a pilot or post injection in addition to the main injection, including parametric sweeps over both the injected mass share and the hydraulic dwell time between injection events. The results provide the following key insights:

Pilot injection strategies:

- DFI showed a 65–70% reduction in soot emissions compared to the FSI configuration across all tested conditions, confirming its low-soot potential even under MI conditions.
- NOx emissions were influenced differently under FSI and DFI operation, with FSI presenting a stronger performance degradation under conditions where the pilot-to-main interaction was stronger, reaching even 25% higher values compared to standalone main case. In contrast, DFI showed a 7% NOx increase in the worst pilot-main tested condition.
- In general, DFI showed a lower sensitivity to the introduction of the pilot injection, which highlights the possibility of using calibrations not suitable for FSI in order, for instance, to reduce both soot and NOx, while maintaining low combustion noise.

Post injection strategies:

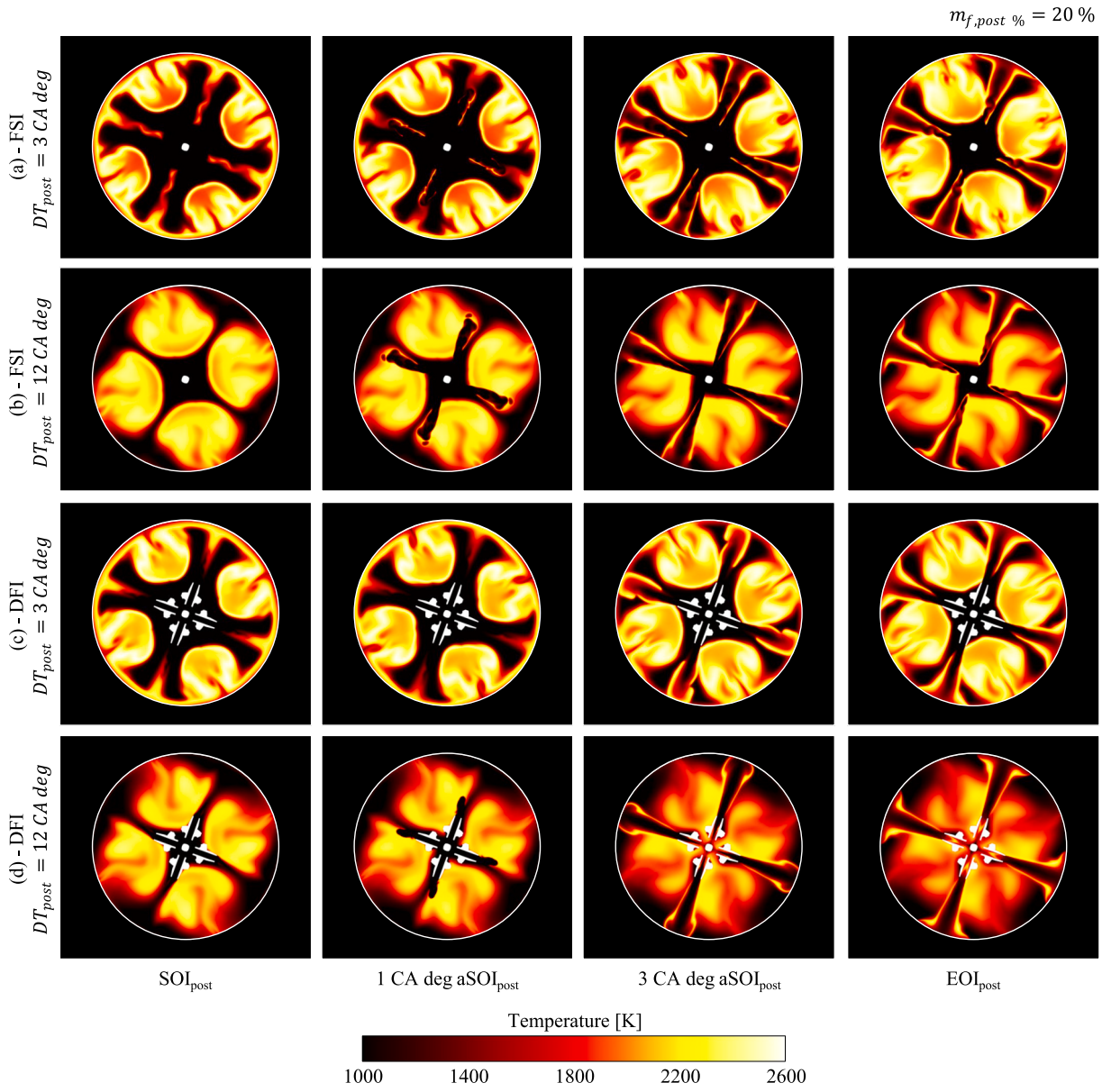


Fig. 14. Temperature distribution on a plane containing the spray axis for the FSI and DFI configurations at different time instants (from left to right), in the case with post-injection featuring $m_{f,post\%} = 20\%$. Results are shown for FSI with $DT_{post} = 3$ CA deg (a) and 12 CA deg (b), and for DFI with $DT_{post} = 3$ CA deg (c) and 12 CA deg (d).

- Both FSI and DFI configurations benefited from significant soot reductions when a post injection was added, confirming the known capability of post injections to mitigate particulate emissions.
- DFI continued to outperform FSI in terms of soot control across all conditions, yielding 50–75% lower soot with a post injection, with simultaneous NOx reductions of 5–10% possible.
- A noticeable sensitivity to dwell time (DT) between main injection and post injection emerged for DFI. The longer the DT, the more time is available for the main flame to recirculate toward the injector tip, which can cause the post injection to ignite in proximity to or even inside the duct. This increases soot formation related to the post injection and curtails part of its advantage on the soot oxidation process. This aspect was not critical for FSI, thus a different optimal calibration is likely needed for DFI.
- In particular, the risk of in-duct combustion increases for high DT (or for very long injection duration in general) due to the possibility of entrainment of hot combustion products rather than fresh air at the duct inlet.

In summary, this study reinforces the advantages of DFI in reducing soot emissions even when coupled with more complex injection strategies. It also highlights the importance of a dedicated calibration of injection parameters when implementing MI strategies in DFI systems, especially in relation to the interaction between closely spaced injection events. Although the extent of the observed phenomena depends on engine operating conditions, engine calibration, and geometrical characteristics, the present findings represent a further step in the understanding and development of DFI and provide a solid basis for future optimization and application of the technology in production diesel engines. Future studies will focus on the optimization of the overall combustion system and on the coupling of DFI with renewable diesel-like fuels, with the ultimate goal of enabling a low-emissions, low-life-cycle-CO_2 solution for heavy-duty compression-ignition engine-based transportation.

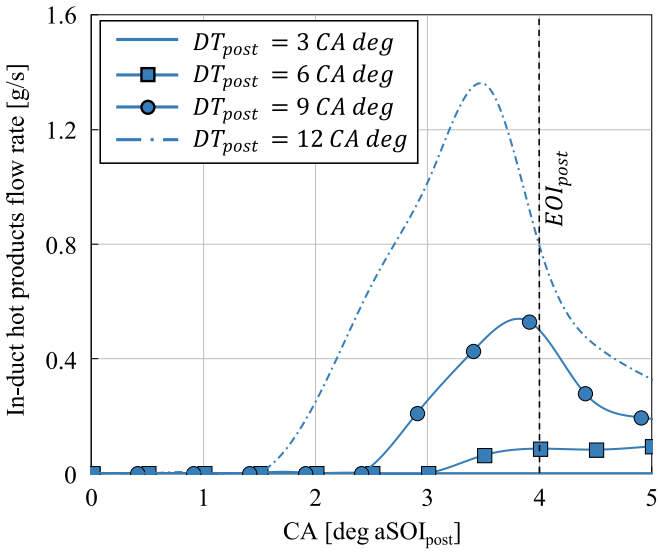


Fig. 15. In-duct entrainment of hot gases for MI cases featuring $m_{f,post\%} = 20\%$ and a $DT_{post} = 3$ CA deg (solid line), $DT_{post} = 6$ CA deg (square-marked solid line), $DT_{post} = 9$ CA deg (circle-marked solid line) and $DT_{post} = 12$ CA deg (dash-dot line).

CRediT authorship contribution statement

M. Orlando: Validation, Software, Methodology, Investigation, Formal analysis, Writing – original draft. **C. Segatori:** Validation, Supervision, Project administration, Methodology, Investigation, Conceptualization, Writing – review & editing. **C. Godbold:** Investigation, Data curation, Writing – review & editing. **C.J. Mueller:** Funding acquisition, Validation, Supervision, Resources, Investigation, Formal analysis, Conceptualization, Writing – review & editing. **F. Millo:** Resources, Supervision, Writing – review & editing. **A. Piano:** Supervision, Project administration, Methodology, Investigation, Conceptualization, Writing – review & editing.

Declaration of competing interest

The authors declare that they have no known competing financial interests or personal relationships that could have appeared to influence the work reported in this paper.

Acknowledgements

The authors acknowledge the CINECA award under the ISCRA initiative, for the availability of high-performance computing resources and support.

Convergent Science provided CONVERGE licenses and technical support for this work.

Sandia National Laboratories is a multi-mission laboratory managed and operated by National Technology & Engineering Solutions of Sandia, LLC (NTESS), a wholly owned subsidiary of Honeywell International Inc., for the U.S. Department of Energy's National Nuclear Security Administration (DOE/NNSA) under contract DE-NA0003525. This written work is authored by an employee of NTESS. The employee, not NTESS, owns the right, title and interest in and to the written work and is responsible for its contents. Any subjective views or opinions that might be expressed in the written work do not necessarily represent the views of the U.S. Government. The publisher acknowledges that the U.S. Government retains a non-exclusive, paid-up, irrevocable, world-wide license to publish or reproduce the published form of this written work or allow others to do so, for U.S. Government purposes. The DOE will provide public access to results of federally sponsored research in accordance with the DOE Public Access Plan.

Data availability

Data will be made available on request.

References

[1] H. Ritchie, Cars, planes, trains: where do CO_2 emissions from transport come from?. https://ourworldindata.org/co2-emissions-from-transport (accessed July 20, 2025).
[2] European Environment Agency, Transport and Mobility. https://www.eea.europa.eu/en/topics/in-depth/transport-and-mobility (accessed July 20, 2025).
[3] Fit for 55: increasing the uptake of greener fuels in the aviation and maritime sectors. https://www.consilium.europa.eu/en/infographics/fit-for-55-refueleu-and-fueleu/ (accessed October 21, 2025).
[4] Fit for 55: why the EU is toughening CO2 emission standards for cars and vans. www.consilium.europa.eu/en/infographics/fit-for-55-emissions-cars-and-vans/ (accessed October 21, 2025).
[5] A.C. Kulzer, Sustainable energy & powertrain solution…based on hydrogen, in: Hydrogen for Sustainable Mobility Forum, Torino, 2025.
[6] F. Leach, G. Kalghatgi, R. Stone, P. Miles, The scope for improving the efficiency and environmental impact of internal combustion engines, Transp. Eng. 1 (2020) 100005, https://doi.org/10.1016/j.treng.2020.100005.
[7] Z. Yue, H. Liu, Advanced research on internal combustion engines and engine fuels, Energies (Basel). 16 (2023) 5940, https://doi.org/10.3390/en16165940.
[8] ourworldindata.org, Share of new cars sold that are battery-electric and plug-in hybrid, 2010 to 2024. https://ourworldindata.org/grapher/share-car-sales-battery-plugin (accessed January 21, 2026).
[9] European Heavy Duty Vehicle Market Development Quarterly (January – March 2025). https://theicct.org/publication/eu-hdv-market-development-quarterly-jan-mar-2025-may25/ (accessed October 21, 2025).
[10] New commercial vehicle registrations: vans -12.2%, trucks -16%, buses -1.8% in Q1 2025. https://www.acea.auto/cv-registrations/new-commercial-vehicle-registrations-vans-12-2-trucks-16-buses-1-8-in-q1-2025/ (accessed October 21, 2025).
[11] IMARC, Marine Propulsion Engine Market Size, Share, Trends and Forecast by Engine Type, Power Source, Power Range, Vessel Type, and Region, 2025-2033. https://www.imarcgroup.com/marine-propulsion-engine-market (accessed January 20, 2026).
[12] C.J. Mueller, C.W. Nilsen, D.J. Ruth, R.K. Gehmlich, et al., Ducted fuel injection: a new approach for lowering soot emissions from direct-injection engines, Appl. Energy 204 (2017) 206–220, https://doi.org/10.1016/j.apenergy.2017.07.001.
[13] C.J. Mueller, Ducted fuel injection, in: U.S. Patent 9,909,549 B2, 2018.
[14] C. Segatori, A. Piano, B. Peiretti Paradisi, A. Bianco, et al., Exploiting the potential of large eddy simulations (LES) for ducted fuel injection investigation in non-reacting conditions, Int. J. Multiphase Flow 171 (2024) 104686, https://doi.org/10.1016/j.ijmultiphaseflow.2023.104686.
[15] F. Millo, A. Piano, B. Peiretti Paradisi, L. Postrioti, et al., Ducted fuel injection: experimental and numerical investigation on fuel spray characteristics, air/fuel mixing and soot mitigation potential, Fuel 289 (2021) 119835, https://doi.org/10.1016/j.fuel.2020.119835.
[16] C.J. Polonowski, C.J. Mueller, C.R. Gehrke, T. Bazynet, et al., An experimental investigation of low-soot and soot-free combustion strategies in a heavy-duty, single-cylinder, direct-injection, optical diesel engine, SAE Int. J. Fuels Lubr. 5 (2011), https://doi.org/10.4271/2011-01-1812, 2011-01–1812.
[17] C. Godbold, I. Gupta, E. Kurtz, C.J. Mueller, et al., Experimental investigation of mixing phenomena for ducted fuel injection, Proc. Combust. Inst. 40 (2024) 105385, https://doi.org/10.1016/j.proci.2024.105385.
[18] C.J. Mueller, C.W. Nilsen, D.E. Biles, B.F. Yraguen, Effects of fuel oxygenation and ducted fuel injection on the performance of a mixing-controlled compression-ignition optical engine with a two-orifice fuel injector, Appl. Energy Combust. Sci. 6 (2021) 100024, https://doi.org/10.1016/j.jaecs.2021.100024.
[19] G. Nyrenstedt, C.W. Nilsen, D.E. Biles, C.J. Mueller, Ducted fuel injection with low-net-carbon fuels as a solution for meeting future emissions regulations, Fuel 338 (2023) 127167, https://doi.org/10.1016/j.fuel.2022.127167.
[20] K. Svensson, R. Fitzgerald, G. Martin, Ducted fuel injection: confirmed re-entrainment hypothesis, WCX SAE World Congress Experience, Detroit, Michigan, United States, April 16, 2024, https://doi.org/10.4271/2024-01-2885.
[21] J.V. Pastor, C. Micó, F. Lewiski, U. Bin-Khalid, Evaluation of the ducted fuel injection concept for medium duty engines and multi-hole nozzles: an optical analysis, Appl. Energy 376 (2024) 124305, https://doi.org/10.1016/j.apenergy.2024.124305.
[22] A. Piano, C. Segatori, F. Millo, F. Pesce, et al., Investigation of ducted fuel injection implementation in a retrofitted light-duty diesel engine through numerical simulation, SAE Int. J. Engines 16 (5) (2023) 643–661, https://doi.org/10.4271/03-16-05-0038.
[23] Conference Report: SAE WCX 2025 Congress. https://dieselnet.com/news/2025/04sae_wcx.php (accessed October 21, 2025).
[24] R. Ogren, K. Baumgard, V. Radhakrishna, R. Kempin, et al., First investigation of ducted fuel injection on a retrofitted heavy-duty multi-cylinder production engine, SAE Int. J. Fuels Lubr. 19 (1) (2026) 83–108, https://doi.org/10.4271/04-19-01-0005.

[25] M. Dürnholz, H. Endres, P. Frisse, Preinjection a measure to optimize the emission behavior of DI-diesel engine, International Congress & Exposition, Detroit, Michigan, United States, February 28, 1994, https://doi.org/10.4271/940674.
[26] G. Stumpp, M. Ricco, Common rail - an attractive fuel injection system for passenger car DI diesel engines, International Congress & Exposition, Detroit, Michigan, United States, February 26, 1996, https://doi.org/10.4271/960870.
[27] S.S. Busch, K. Zha, P. Miles, A. Warey, et al., Experimental and numerical investigations of close-coupled pilot injections to reduce combustion noise in a small-bore diesel engine, SAE Int. J. Engines 8 (2) (2015) 660–678, https://doi.org/10.4271/2015-01-0796.
[28] T. Tanaka, Study on pilot injection of DI diesel engine using common-rail injection system, JSAE Rev. 23 (2002) 297–302, https://doi.org/10.1016/S0389-4304(02)00195-9.
[29] J. O'Connor, M. Musculus, Post injections for soot reduction in diesel engines: a review of current understanding, SAE Int. J. Engines 6 (1) (2013) 400–421, https://doi.org/10.4271/2013-01-0917.
[30] X. Liu, H.G. Im, C.J. Mueller, G. Nyrenstedt, A computational parametric study of ducted fuel injection implementation in a heavy-duty diesel engine, Fuel 358 (2024) 130228, https://doi.org/10.1016/j.fuel.2023.130228.
[31] Z. Wang, T. Liang, Y. Zhang, Z. Wang, Experimental and numerical investigation of ducted spray with dual injection strategies, Atomiz. Sprays 33 (2023) 21–46, https://doi.org/10.1615/AtomizSpr.2023046365.
[32] C. Godbold, C. Segatori, C.J. Mueller, C. Genzale, et al., Impact of pilot injections on ducted fuel injection performance, Int. J. Engine Res. (2026), https://doi.org/10.1177/14680874261426780.
[33] C. Segatori, M. Orlando, A. Piano, F. Millo, et al., Optical diagnostics-based numerical modeling of a compression-ignition optical research engine implementing ducted fuel injection, Appl. Energy Combust. Sci. 24 (2025) 100408, https://doi.org/10.1016/j.jaecs.2025.100408.
[34] C.W. Nilsen, D.E. Biles, B.F. Yraguen, C.J. Mueller, Ducted fuel injection versus conventional diesel combustion: an operating-parameter sensitivity study conducted in an optical engine with a four-orifice fuel injector, SAE Int. J. Engines 13 (2020), https://doi.org/10.4271/03-13-03-0023, 03-13-03–0023.
[35] C.W. Nilsen, D.E. Biles, B.M. Wilmer, C.J. Mueller, Investigating the effects of duct length and diameter and fuel-injector orifice diameter in a compression-ignition engine equipped with ducted fuel injection, Appl. Energy Combust. Sci. 7 (2021) 100030, https://doi.org/10.1016/j.jaecs.2021.100030.
[36] R.K. Gehmlich, C.J. Mueller, D.J. Ruth, C.W. Nilsen, S.A. Skeen, J. Manin, Using ducted fuel injection to attenuate or prevent soot formation in mixing-controlled combustion strategies for engine applications, Appl. Energy 226 (2018) 1169–1186, https://doi.org/10.1016/j.apenergy.2018.05.078.
[37] K.J. Richards, P.K. Senecal, E. Pomraning, CONVERGE 3.1 Manual, Convergent Science, Madison, 2023.
[38] B.E. Launder, B.I. Sharma, Application of the energy-dissipation model of turbulence to the calculation of flow near a spinning disc, Lett. Heat Mass Transf. 1 (1974) 131–137, https://doi.org/10.1016/0094-4548(74)90150-7.
[39] S.B. Pope, An explanation of the turbulent round-jet/plane-jet anomaly, AIAA J. 16 (1978) 279–281, https://doi.org/10.2514/3.7521.
[40] A.A. Amsden, KIVA-3V: A Block-Structured KIVA Program for Engines with Vertical or Canted Valves, Los Alamos, NM, 1997, https://doi.org/10.2172/505339.
[41] Engine Combustion Network (ECN). https://ecn.sandia.gov/ (accessed December 6, 2024).
[42] T. Zeuch, G. Moréac, S.S. Ahmed, F. Mauss, A comprehensive skeletal mechanism for the oxidation of n-heptane generated by chemistry-guided reduction, Combust. Flame 155 (2008) 651–674, https://doi.org/10.1016/j.combustflame.2008.05.007.
[43] J.B. Heywood, Internal Combustion Engine Fundamentals, McGraw-Hill Book Company, New York, 1988. ©1988, 1998, https://search.library.wisc.edu/catalog/999610484402121.
[44] A. Kazakov, M. Frenklach, Dynamic modeling of soot particle coagulation and aggregation: implementation with the method of moments and application to high-pressure laminar premixed flames, Combust. Flame 114 (1998) 484–501, https://doi.org/10.1016/S0010-2180(97)00322-2.
[45] C. Nilsen, D. Biles, C.J, C. Mueller, Using ducted fuel injection to attenuate soot formation in a mixing-controlled compression ignition engine, SAE Int. J. Engines 12 (3) (2019) 309–322, https://doi.org/10.4271/03-12-03-0021.
[46] C. Nilsen, D. Biles, B. Yraguen, C.J. Mueller, Ducted fuel injection vs. conventional diesel combustion: extending the load range in an optical engine with a four-orifice fuel injector, SAE Int. J. Engines 14 (1) (2021) 47–58, https://doi.org/10.4271/03-14-01-0004.
[47] M. Badami, F. Mallamo, F. Millo, E. Rossi, Influence of multiple injection strategies on emissions, combustion noise and BSFC of a DI common rail diesel engine, in: SAE Technical Paper 2002-01-0503, 2002, https://doi.org/10.4271/2002-01-0503.
[48] Z. Han, A. Uludogan, G. Hampson, R. Reitz, Mechanism of soot and NOx emission reduction using multiple-injection in a diesel engine, SAE Technical Paper 960633 (1996), https://doi.org/10.4271/960633.
[49] F. Millo, A. Piano, B. Peiretti Paradisi, C. Segatori, et al., Ducted fuel injection: a numerical soot-targeted duct geometry optimization, SAE Int. J. Engines 15 (2) (2022) 297–317, https://doi.org/10.4271/03-15-02-0014.